Groundwater Monitoring&Remediation

Infiltration of Sulfate to Enhance Sulfate-Reducing Biodegradation of Petroleum Hydrocarbons

by Yunxiao Wei, Neil R. Thomson, Ramon Aravena, Massimo Marchesi, James F. Barker, Eugene L. Madsen, Ravi Kolhatkar, Tim Buscheck, Daniel Hunkeler, Christopher M. DeRito

Abstract

The lack of sufficient electron acceptors, particularly sulfate, can limit the rate of biodegradation of petroleum hydrocarbons (PHCs). Hence, there is a growing interest by remediation practitioners to deliver sulfate to a PHC impacted saturated zone to enhance biodegradation. When shallow contamination is present in a relatively permeable aquifer and site constraints allow, a cost-effective approach is to apply sulfate on the ground surface. In this investigation a pilot-scale experiment was conducted to increase our understanding of the delivery of sulfate using a surface-based method and the resulting impact on a shallow PHC contaminated aquifer. A surficial infiltration pond positioned on the ground surface above a well-characterized residual PHC source zone was used to control sulfate dosing. A high-resolution network near the infiltration pond and downgradient of the source zone was employed to monitor relevant geochemical indicators and PHC concentrations. Compound-specific isotope analysis (CSIA) was used to identify biodegradation patterns and to investigate the occurrence of microbial sulfate reduction. Selected metabolites and reverse-transcriptase quantitative polymerase chain reaction analyses of expressed biodegradation genes (as mRNA) were also used to characterize the response of indigenous microorganisms (especially sulfate-reducing bacteria) to the added sulfate. Three sulfate application episodes (5000 L each) at various Na_2SO_4 concentrations were allowed to infiltrate under a constant hydraulic head. Although the applied sulfate solution was impacted by density-driven advection, detailed monitoring data indicated that the sulfate-enriched water mixed with upgradient groundwater as it migrated downward through the residual PHC zone and formed a co-mingled downgradient plume with the dissolved PHC compounds. The enrichment of $\delta^{34}S$ of sulfate in conjunction with a decrease in sulfate concentration showed the occurrence of sulfate reduction due to the applied sulfate. Increased dissolved inorganic carbon (DIC) concentrations associated with a shift toward more depleted values of $\delta^{13}C$ of DIC was indicative of an input of isotopically depleted DIC from biodegradation of PHCs. Despite fluctuations in benzene, toluene, and *o*-xylene (BTX) concentrations, the CSIA data for BTX showed that these compounds were biodegraded. The biomarker data provided supporting evidence that toluene and *o*-xylene were undergoing anaerobic biodegradation due to sulfate reduction. This study provides insight into factors controlling surface-based delivery of sulfate to shallow PHC impacted groundwater systems, and the value of isotopic and molecular-biological procedures to augment conventional monitoring tools.

Introduction

At sites contaminated with petroleum hydrocarbons (PHCs), biodegradation is often one of the most important attenuation mechanisms that contribute to the reduction in contaminant mass in both the source zone and dissolved PHC plumes. Since dissolved oxygen (DO) is rapidly consumed and the rate of oxygen supply is not able to meet the aerobic biodegradation demand, anaerobic conditions usually develop. Anaerobic biological oxidation of PHCs is widespread (Atlas 1981; Leahy and Colwell 1990; Chapelle 1999; Foght 2008; Meckenstock and Mouttaki 2011) and commonly leads to depleted concentrations of alternative electron acceptors (EAs; e.g., nitrate, ferric iron, and sulfate) in groundwater plumes. This lack of sufficient EAs can limit the rate of biodegradation of PHCs (Meckenstock et al. 2015). To overcome this limitation, engineered systems that deliver selected soluble EAs have been applied in anaerobic environments to stimulate biodegradation of PHCs (Lunardini Jr. and Dickey III 2003; Suthersan et al. 2011). Although nitrate and ferric iron have been shown to be more effective than sulfate by Cunningham et al. (2001), these are less desirable EAs as the regulatory maximum contaminant level (MCL) for nitrate in groundwater is only 44 mg/L, and ferric iron is not practical due to its low solubility at neutral aquifer pH (Cunningham et al. 2001). Sulfate has been estimated to account for about 70% of the overall natural biodegradation capacity (Wiedemeier et al. 1999) in PHC groundwater plumes, which consequently gives rise to sulfate depleted conditions in these systems (Roychoudhury and McCormick 2006; U.S. EPA 2007; Kolhatkar and Schnobrich 2017). Therefore, there has been

Article impact statement: CSIA and biomarkers used to evaluate enhanced biodegradation of PHCs resulting from surface-based delivery of sulfate.

 doi: 10.1111/gwmr.12298

a growing interest in sulfate addition at sites impacted with PHCs to enhance the biodegradation of PHCs.

Various approaches have been used to deliver a sulfate solution to the saturated zone including gravity feed into injection wells (Anderson and Lovley 2000; Kolhatkar et al. 2008), a series of injection and extraction wells (Cunningham et al. 2001), and gravity feed into an infiltration trench (Sublette et al. 2006). The results from these studies clearly demonstrated the effectiveness of stimulating PHC biodegradation in the vicinity of the delivery location, but indicated various limitations with approaches to deliver a sulfate solution. These included a limited zone of influence downgradient of the injection point (either due to short-circuiting along the more permeable strata or density-driven advection of the concentrated injected sulfate solution) and difficulty in maintaining a relatively uniform sulfate concentration over time. As a result, the direct delivery of a sulfate solution to the saturated zone is associated with higher costs to satisfy closely spaced injection locations and/or more frequent sulfate delivery events.

An alternative approach is to deliver sulfate from the land surface. Hutchins and Miller (1998) used a sprinkler application system with and without nitrate addition on adjacent 30×30 m experimental plots, and compared the extent of bioremediation of a JP-4 fuel contaminated aquifer. Based on the changes in groundwater and soil core concentrations of benzene, toluene, ethylbenzene, xylene (BTEX), and trimethylbenzenes (TMBs), they demonstrated an approximately fivefold increase in mass removal in the nitrate plot relative to the plot without nitrate addition. A number of studies have also demonstrated the important role of natural surface recharge in transporting rate-limiting nutrients and EAs to groundwater. This process has been shown to exert an important control on natural attenuation of dissolved contaminants (McGuire et al. 2005; van Stempvoort et al. 2007), as well as methanogenic biodegradation of long chain alkanes in a crude oil body located in the shallow subsurface (Bekins et al. 2005; Baedecker et al. 2018).

Based on these efforts, there is an increased interest in applying a "*surface delivery*" method of EAs over the entire footprint of a PHC plume as a cost-effective approach to enhance biodegradation of PHCs, especially at open/unpaved sites with shallow contamination in a relatively permeable aquifer. Kolhatkar and Schnobrich (2017) described pilot testing and subsequent site-wide land application of agricultural gypsum and Epsom salt followed by irrigation or natural precipitation to provide sulfate to a predominantly benzene plume in a shallow groundwater system. At this site, up to a threefold increase in the rate of benzene attenuation was demonstrated at some monitoring wells following land application events where elevated sulfate concentrations (>150 mg/L) were sustained over 12 months. Despite these enhancements, they identified the need to better understand factors controlling sulfate infiltration to groundwater, and the desire for novel diagnostic tools to optimize the performance of these systems.

To improve our understanding of the delivery of sulfate using a surface method and the resulting impact on a shallow PHC contaminated aquifer, a pilot-scale experiment was designed and executed. While land application of solid sulfate salts (gypsum or Epsom) is likely more cost-effective, it involves an additional step and potential rate limitations associated with the dissolution of the salt. To eliminate this uncertainty, the sulfate dose in this experiment was delivered episodically using a surficial infiltration pond positioned above a well-characterized PHC residual source zone. The objectives of this experiment were: (1) to assess the spatial and temporal distribution of sulfate in groundwater and associated changes in PHC concentrations and (2) to augment conventional groundwater parameters with isotopic and molecular-biological procedures to evaluate potential enhanced biodegradation of PHCs resulting from the applied sulfate. A high-resolution monitoring network consisting of multiple transects of depth-discrete sampling points was employed to capture the behavior of the infiltrating sulfate. Geochemical indicators included DO, electrical conductivity (EC), redox potential (Eh), pH, dissolved inorganic carbon (DIC) content, methane, and sulfide. These data were enhanced with compound-specific isotope analysis (CSIA) and biomarkers (GC/MS analysis of metabolites and quantitative polymerase chain reaction [qPCR] methods of expressed biodegradation genes).

Methods

Site Description

This study was performed in an experimental gate (Figure 1) previously used by Freitas et al. (2011) located in the sandpit area of the University of Waterloo Groundwater Research Facility at the Canadian Forces Base (CFB) in Borden, ON, Canada. The Borden aquifer material is considered homogenous and is composed of well-sorted fine to medium grain sand (hydraulic conductivity 6.0×10^{-6} to 2.0×10^{-4} m/s) with some microscale heterogeneity in the form of silty sand and coarse sand lenses (Mackay et al. 1986). The water table is usually located at ~1 m below ground surface (bgs) but varies seasonally, and the horizontal groundwater flow velocity is ~9 cm/day. The underlying aquitard is ~8 m thick and located at ~11 m bgs. A historical leachate plume exists >5 m bgs and is responsible for the background concentration of SO_4^{2-} (10 to 30 mg/L), and Na^+ (1 to 2 mg/L) starting at about 4.5 m bgs (MacFarlane et al. 1983). This experimental gate is bounded by sheet pile walls that are parallel to the nominal groundwater flow direction. As a result, groundwater flow within this gate is controlled by the ambient aquifer flow conditions.

Approximately 12 months before this field investigation began, 112 L of a well-characterized PHC mixture (Table S1, Supporting Information) was injected from 1.25 to 2.5 m bgs between Rows 2 and 3 (Figure 1a). Twelve stainless-steel drive points were driven down to 2.25 m bgs, and then 2.5 L aliquots of the mixture were injected at predetermined depth intervals before each drive point was pulled upwards to the next interval. Following injection, the water table in the gate was lowered to 2.5 m bgs and allowed to recover ~12 times over a 7-day period to generate a smear zone. Based on a qualitative assessment of the PHC distribution using an ultraviolet optical screening tool (UVOST; Dakota Technologies, Fargo, North Dakota) the footprint of the residual source was approximately 3×3 m and extended vertically from 0.8 to 2.8 m bgs (see Figure S1).

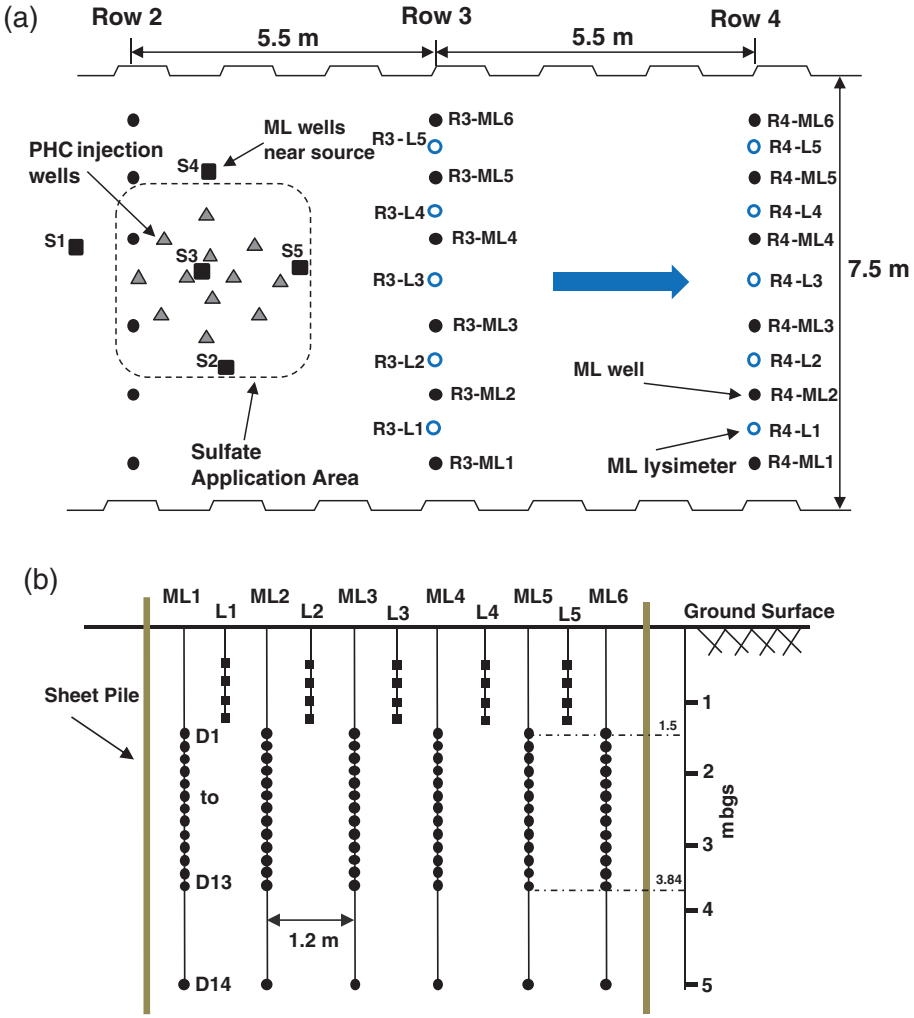

Figure 1. (a) Plan view of a portion of the experimental gate located in the sandpit area at CFB Borden showing the location of the monitoring infrastructure, PHC injection wells, and the spatial extent of the sulfate infiltration pond; and (b) cross-sectional view looking upgradient at one of the monitoring rows showing the location of the monitoring points.

Monitoring Infrastructure

The relevant monitoring network consisted of three groundwater monitoring transects or fences identified as Rows 2, 3, and 4 installed 5.5 m apart (Figure 1a). Each transect contained six multilevel monitoring wells (ML1 to ML6) separated by 1.2 m. Each ML well was equipped with 14 sampling locations (10 cm long screened interval). The upper 13 locations were evenly distributed from 1.50 to 3.84 m bgs at 0.19 m intervals (D1 to D13), and the deepest location (D14) was screened between 4.8 and 5.3 m bgs (Figure 1b). Each sampling location is denoted by a row number, multilevel monitoring well number, and sampling interval. For example, R3-ML4-D3 identifies a monitoring location in Row 3 (R3), multilevel well 4 (ML4) at the third depth interval (D3). To complement the monitoring transects, five additional multilevel monitoring wells (identified as source monitoring wells S1 to S5) were installed within and adjacent to the residual PHC source zone (Figure 1a). Each of these monitoring wells was equipped with eight sampling locations screened from 0.5 to 4.0 m bgs at 0.5 m intervals (denoted as Sx-D1 to Sx-D8).

To monitor the unsaturated zone, 10 suction lysimeters, identical to those used by Freitas and Barker (2008), were installed along the Rows 3 and 4 transects (Figure 1a). Each lysimeter was comprised of four sampling locations screened at a nominal depth of 0.50, 0.75, 1.00, and 1.25 m bgs (Figure 1b). Each lysimeter sampling location is denoted by row number (R3 or R4), lysimeter number (L1 to L5), and sampling interval (D1 to D4).

Sulfate Application System

To remove potential uncertainties associated with a land surface sulfate application system that relied on natural or artificial precipitation as the driving force, we chose to use a surficial infiltration pond to control sulfate application volume, concentration, and timing. A 3.25×3.25 m infiltration pond was constructed from 0.15-m-wide×0.05-m-thick wood planks and centered over the footprint of the residual PHC source zone (Figure 1a). Natural vegetation was removed from the interior of the pond, and the soil surface was raked by hand to a depth of ~5 cm to increase the likelihood of uniform infiltration below the pond. Nearby soil material was used to build a berm around on the exterior of the pond structure (Figure 2).

A total of three sulfate solution applications were planned. To assist with determining the initial system design parameters (i.e., ponding depth, total volume, and sulfate concentration), a series of three-dimensional density-dependent flow

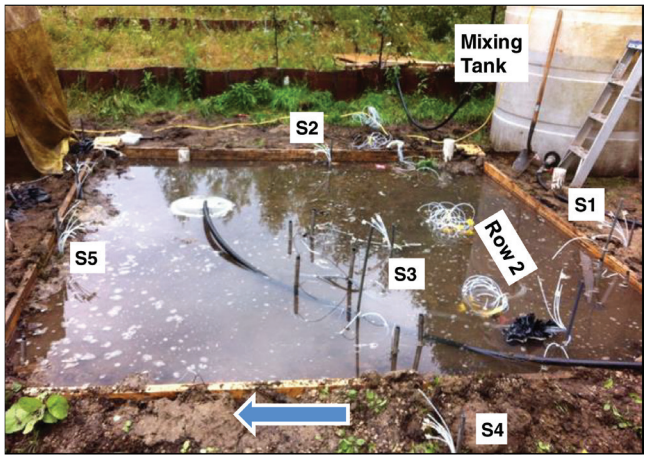

Figure 2. Image of the sulfate infiltration pond with a constant water level during an application episode. Multilevel source monitoring wells S1 to S5 are indicated. Since this image was taken looking from the top of Figure 1a toward the infiltration pond, groundwater flow is from right to left as indicated by the arrow.

and mass transport simulations using SALTFLOW (Molson and Frind 2013) were performed. A key design consideration was the sulfate concentration since this controls density-driven advection and the ability of the infiltrating solution to penetrate into and through the source zone. Based on the simulation results, it was estimated that 5000 L of a 5 g/L Na_2SO_4 solution released in the infiltration pond at a ponding depth of 0.1 m would migrate through the source zone in ~40 days. These parameters were adopted for the initial (Day 0) application (Episode 1). The parameters of the two subsequent application episodes were adjusted based on the data collected. It was by no means the attempt of this pilot-scale experiment to deliver sufficient sulfate for complete treatment of the source zone mass.

The sulfate solution was prepared, in batches, in a 3780 L tank using uncontaminated groundwater extracted from a nearby well and Na_2SO_4 solids (Kissner Milling Co. Ltd., Cambridge, Ontario, Canada) (Figure 2). Each batch was prepared and allowed to mix using a submersible pump recirculation system for at least 8 h before use. A 15-m length of 3.8-cm diameter tubing was used to transfer the sulfate solution from the tank to the infiltration pond. The dispensing flow rate was controlled by a gate valve at the outlet of the tank which was manually adjusted to maintain a constant water level in the pond. The position of the drainage outlet was changed every ~20 min to evenly distribute the sulfate solution across the pond. The sulfate solution was allowed to infiltrate into the subsurface under a controlled ponding depth of 0.1 m.

Sampling and Analyses

To follow the migration and fate of the applied sulfate and the dissolved PHC compounds, we focused our attention on the sampling locations across Rows 3 and 4, and the source monitoring wells. Groundwater samples from these locations were used to determine EC, and the concentration of sulfate and the PHC compounds. To monitor for the potential enhanced biodegradation of PHCs by sulfate reduction, 5 locations in the source monitoring wells, 5 locations across the Row 3 transect, and 10 locations across the Row 4 transect were selected. These 20 locations were between 0.5 and 3 m bgs and chosen based on the anticipated migration pathway of the released sulfate from the infiltration pond and through the PHC source. In addition to EC and the concentration of sulfate and the PHC compounds, groundwater samples from these 20 locations were also analyzed for pH, DO, oxidation reduction potential (Eh), sulfide, methane, DIC, ^{34}S of sulfate, ^{13}C of DIC, and CSIA ($\delta^{13}C$ and $\delta^{2}H$) of benzene, toluene, and *o*-xylene. Furthermore, biomarkers characteristic of selected reactions were analyzed including mRNA of functional genes and metabolites. Specifically, we focused on a total of four metabolites that are uniquely of microbial origin: benzene cis-dihydrodiol indicative of aerobic benzene degradation, toluene cis-dihydrodiol indicative of aerobic toluene degradation, benzylsuccinate indicative of anaerobic toluene degradation, and 2-methylbenzylsuccinate indicative of anaerobic xylene degradation (Wilson and Madsen 1996; Gülensoy and Alvarez 1999; Beller et al. 2008; Cébron et al. 2008; Nebe et al. 2009; Fuchs et al. 2011; Diaz et al. 2013). Detection of mRNA of biodegradation genes shows that microorganisms hosting the DNA encoding the biodegradation enzymes are metabolically active and engaged in the biodegradation process. The *todC* (aromatic dioxygenase) genes can be positive during the biodegradation of benzene or toluene under aerobic conditions (Hendrickx et al. 2006; Cébron et al. 2008; Nebe et al. 2009). The *abcA* gene (anaerobic benzene carboxylase) is characteristic of benzene biodegradation under iron-reducing and other anaerobic conditions (Abu Laban et al. 2010). The *bssA* gene (and corresponding mRNA) encodes biodegradation of toluene and xylene under anaerobic conditions (Kazy et al. 2010; Fuchs et al. 2011). A specific variant of the *bssA* gene, *bssA*-SRB, has been shown to be carried by bacteria that are active in anaerobic toluene metabolism under sulfate-reducing conditions (Beller et al. 2008). Therefore, detecting mRNA of the *bssA*-SRB gene links biodegradation of toluene to populations carrying out sulfate reduction. Finally, respiratory reduction of sulfate in anaerobic conditions has been linked to the expression of the beta subunit of

the dissimilatory (bi)sulfite reductase genes, *dsrB* (Neretin et al. 2003; Geets et al. 2006; Chin et al. 2008; Bourne et al. 2011; Pelikan et al. 2016).

A peristaltic pump and a sampling manifold (Mackay et al. 1986) was used to collect groundwater samples from the multilevel locations. Prior to collecting samples, ~60 mL was purged from each sampling point to flush the water inside the tubing and the sampling manifold. Samples collected for sulfate and sulfide analyses were filtered with a 0.45 µm syringe membrane filter, and acidified with nitric acid (Sigma-Aldrich, St. Louis, Missouri) to a pH < 2. Samples for DIC, PHCs and for CSIA analyses were collected in 40-mL glass vials and preserved with 0.5 mL of a 10% sodium azide solution. Samples for isotope analysis (^{34}S) of sulfate were collected in 1-L glass bottles without addition of preservatives. Samples for ^{13}C analysis of DIC were collected in 60-mL transparent glass bottles with 0.2 mL of saturated mercuric chloride solution added for sterilization. Samples for analysis of metabolites were collected in two 500-mL glass bottles; one bottle was preserved by adding HCl (J.T. Baker, Phillipsburg, New Jersey) to a target pH of <2, and the other bottle was preserved with NaOH (Fisher Scientific, Fair Lawns, New Jersey) to a target pH of ~8. All samples were stored at 4 °C and held for up to 14 days prior to analyses. The samples for qPCR analyses were collected by passing 2 L of groundwater through a 0.2-µm Sterivex filter. The filter was then frozen immediately and stored at −80 °C until further processing.

Details of the analytical methods used to: (1) quantify the concentration of organic compounds and inorganic species; (2) analyze carbon ($^{13}C/^{12}C$), hydrogen ($^{2}H/^{1}H$), and sulfur ($^{34}S/^{32}S$) isotope ratios; (3) extract and analyze DNA and RNA from groundwater biomass; and (4) identify specific metabolites are provided in Appendix S1.

Results and Discussion

Figure 3a conceptually illustrates the anticipated behavior of this experimental investigation to enhance sulfate reduction within and downgradient of the PHC source. For ~12 months before sulfate was applied, the residual PHC source was allowed to produce dissolved plumes of the various PHC compounds, and to promote favorable conditions for the acclimation and growth of indigenous sulfate-reducing bacteria (SRB). SRB communities capable of complete oxidation of benzene, toluene and xylene have been previously identified (Beller et al. 1996; Harms et al. 1999; Kleikemper et al. 2002). The rate of microbial sulfate reduction is a function of the SRB-specific growth rate which is controlled by the availability of sulfate and the organic substrate used by the microorganisms during energy production (Roychoudhury and McCormick 2006).

Each sulfate application episode was expected to generate a zone of infiltrating sulfate that would intersect the source zone, mix with the developing PHC plumes, and once the short-term hydraulic effects of the ponded infiltration system subsided, migrate downgradient through Row 3 and Row 4 transects. Between each episode, the natural infiltration processes due to rainfall or snowmelt are expected to wash any remnant sulfate held in the unsaturated zone below the infiltration pond into the groundwater system. The increased sulfate concentration was expected to enhance sulfate reduction and lead to a decrease in the concentration of some PHCs and sulfate, and an increase in the concentration of sulfide and DIC (Figure 3b). It is expected that the remaining PHCs (e.g., benzene) would be enriched in ^{13}C and ^{2}H, and sulfate in ^{34}S and ^{18}O, while the DIC produced would be depleted in ^{13}C. Biomarker evidence for increased sulfate reduction was expected to include an increase in *dsrB* transcript levels. As PHCs began

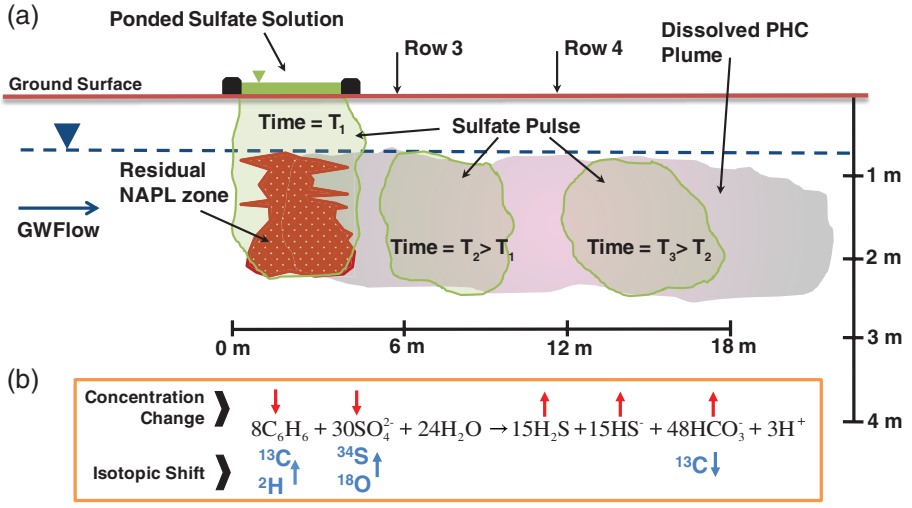

Figure 3. (a) Conceptual schematic of the sulfate delivery method used in this experimental investigation to enhance sulfate reduction within and downgradient of the PHC residual source. The sulfate solution is applied in pulse mode to a bermed-off pond and allowed to infiltrate under gravity. As the sulfate-rich water migrates through the source zone, PHC mass will dissolve. This groundwater will eventually migrate under ambient conditions once the short-term hydraulic effects of the ponded infiltration system have subsided. (b) We hypothesis that the increased sulfate concentration will enhance sulfate reduction and lead to a decrease (↓) in the concentration of some PHCs (e.g., benzene) and sulfate, and an increase (↑) in the concentration of sulfide, and DIC. The remaining benzene will be enriched (↑) in ^{13}C and ^{2}H, and sulfate in ^{34}S and ^{18}O, while the DIC produced will be depleted (↓) in ^{13}C.

to be biodegraded under anaerobic conditions enhanced by sulfate addition, transcripts encoding *abcA* and *bssA*-SRB were expected to increase as were the concentration of the metabolites of toluene (benzylsuccinate) and xylene (methylbenzylsuccinate).

The three sulfate application episodes were conducted on Days 0, 59, and 277. All episodes involved the infiltration of 5000 L of solution; however, the Na_2SO_4 concentration was increased from 5 to 20 g/L for Episode 2, and then reduced to 15 g/L for Episode 3. The variation in Na_2SO_4 concentration was in response to observed density-driven advection of the infiltrating sulfate solution. During and shortly after each application episode, changes to the water table were manually monitored using four wells (screened from 1.5 to 2.0 m bgs; not shown in Figure 1) located just outside the infiltration pond. In general, the water table rose rapidly within the first 60 min and then stabilized. The time for complete infiltration of the 5000 L was 18 h for Episode 1, 14 h for Episode 2, and 24 h for Episode 3. Episode 3 was conducted under spring conditions, and as a result the water table was close to ground surface and hence the infiltration rate was reduced. A baseline sampling event was conducted on Day −1, although groundwater samples were collected on Day −17 from Row 2 for organic compound analysis and these data are shown where appropriate. Following each sulfate application episode, groundwater samples were collected from all locations across Rows 3 and 4 on Days 23, 37, 58, 86, 103, 294, and 394 for EC and/or sulfate analyses. Samples were collected and analyzed from the 20 selected locations to monitor for enhanced biodegradation of PHCs by sulfate reduction on Days 44, 103, and 233.

Sulfate Migration

The baseline sulfate concentration was <20 mg/L and EC < 400 µS/cm as determined from all source monitoring well sampling locations, and across Row 3 and Row 4 transects. The EC of the applied sulfate solution was 6800, 23,500, and 17,700 µS/cm for each of the three application episodes, respectively. The ensemble data set of groundwater samples where EC and sulfate concentration were determined showed a linear relationship ($r^2 = 0.89$) between EC and sulfate (Figure S2) indicating that EC can be used as quantitative indicator of sulfate concentration in this investigation. In the discussion below we use the phrase "equivalent sulfate concentration" to indicate that the sulfate concentration was estimated from EC using the relationship shown in Figure S2.

Following the first application episode, the front of the sulfate plume reached a depth of ~1.5 m bgs by Day 10 directly beneath the infiltration pond at S3-D3 but was not detected at Row 3 (data not shown). By Day 23, there was no change in the depth of penetration beneath the infiltration pond (maximum observed equivalent sulfate concentration of 2250 mg/L at S3-D2), but elevated EC (equivalent sulfate concentration of ~330 mg/L) was observed at Row 3 (Figure 4a) to a depth ~2.0 m bgs suggestive of a slight downward flow component of the sulfate plume. On Day 37 the EC data indicated that the majority of sulfate had left the source zone with moderate EC (equivalent sulfate concentration of ~400 mg/L) detected beneath the source zone (i.e., at S3-D2) (data not shown). At Row 3, the distribution of elevated sulfate had expanded both horizontally and vertically with a core equivalent sulfate concentration of ~3700 mg/L (Figure 4b), compared to the Day 23 distribution (Figure 4a). About 20 days later on

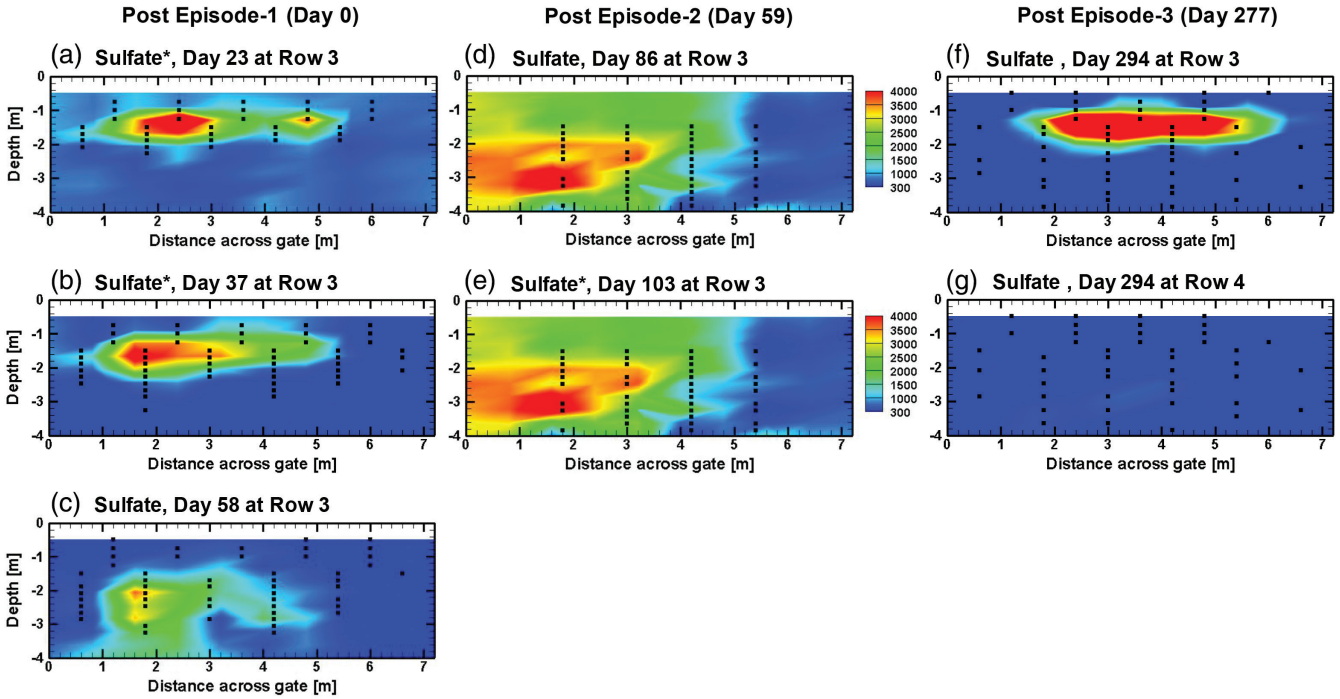

Figure 4. Spatial distribution of sulfate concentration (mg/L) at Rows 3 and 4 looking upgradient following: Episode 1 at (a) Day 23, (b) Day 37, and (c) Day 58; Episode 2 at (d) Day 86 and (e) Day 103; and Epiosde 3 at (f, g) Day 294. The superscript * indicates that the sulfate distribution was estimated from the EC distribution using the relationship shown in Figure S2.

Day 58, moderate sulfate concentrations (up to 1300 mg/L) were still present at a depth of 1.5 m bgs near the downgradient margin of the source zone (S5-D3) (data not shown). The Row 3 sulfate distribution (Figure 4c) on Day 58 indicated that the sulfate concentrations generally increased and sulfate had infiltrated deeper than the Day 37 distribution. The maximum sulfate concentration in the core of the distribution was 4650 mg/L. As expected, no elevated EC was observed at Row 4 on Day 58. In summary, the sulfate distribution resulting from Episode 1 extended to a depth of 1.5 m bgs coincident with the upper portion of the PHC source zone, was asymmetrical, and reached Row 3 in ~20 days.

In an attempt to increase the depth of sulfate penetration into the residual PHC zone for application Episode 2, the Na_2SO_4 concentration was increased to 20 g/L; four times higher than in the first application. On Day 86 (27 days after the second application) the EC data indicated that the infiltration depth of the sulfate-rich water had reached 2.5 m bgs within the source zone (data not shown). This is ~1 m deeper than observed during the first application episode. The Row 3 sulfate distribution at Day 86 (Figure 4d) showed a thin core at ~1.8 m bgs that was 2.5-m wide and 0.5-m thick with concentrations between 4000 and 6000 mg/L. Below the core of this distribution was a region with sulfate concentrations as high as 1500 mg/L that extended to a depth of ~4.0 m bgs. Elevated sulfate concentrations were more widespread and deeper compared to those from the first sulfate application as a result of density-driven migration. No elevated EC or sulfate concentrations were observed at Row 4 on Day 86. By Day 103 (44 days after the second application) the EC data from Row 3 (Figure 4e) indicated that sulfate had spread across most of this monitoring transect with equivalent sulfate concentrations ranging from 1300 to 2900 mg/L. The maximum equivalent sulfate concentration of ~3890 mg/L was observed at a depth of ~3.0 m bgs. This distribution suggested that the applied sulfate likely sank below the monitored depth of ~5 m bgs at Row 3. An elevated sulfate signature from Episode 1 was expected to be observed at Row 4 between Days 90 and 120 based on an assumed groundwater velocity of 9 cm/d; however, no elevated EC was observed at Row 4 on Day 103 likely due, in part, to the sinking of sulfate deeper than the monitoring depth locations.

To reduce the density-driven migration of the applied sulfate observed following Episode 2, the Na_2SO_4 concentration was decreased from 20 to 15 g/L for Episode 3. Figure 4f shows by Day 294 (17 days after the third application) that the core of the sulfate distribution at Row 3 was at a depth of ~1.5 m bgs. This core was symmetric and had elevated sulfate concentration values between 4000 and 6000 mg/L that covered a region that was 3.5-m wide and 1.5-m thick. The maximum sulfate concentration observed across Row 4 at Day 294 was ~470 mg/L at a depth of 3.6 m bgs (Figure 4g). Above this depth, elevated sulfate concentrations were present across Row 4, but the depth of the core of this distribution confirmed sinking of sulfate likely related to Episode 2.

Figure 5 depicts the maximum spatial extent of the sulfate distribution from the data assembled from the three sulfate application episodes. As discussed above, the sulfate-enriched water left the infiltration pond and mixed with upgradient groundwater as it migrated downward through the residual PHC zone. Due to density effects, the sulfate continued to sink and by Row 4 it was observed to reach a depth of ~3.7 m bgs. Based on this distribution, data from 4 of the 20 locations monitored to assess for enhanced biodegradation of PHCs by sulfate reduction were selected for presentation and discussion (Figure 5). Two locations were located at S5 just downgradient of the infiltration pond (i.e., S5-D2 at a depth of 1.0 m bgs, and S5-D3 at a depth of 1.5 m bgs), and the other two locations were in the center of the Row 3 transect (i.e., R3-ML4-D1 at a depth of 1.5 m bgs, and R3-ML4-D3 and a depth of 1.9 m bgs). These four locations are where elevated concentrations of sulfate and PHC compounds were observed to be present during this investigation.

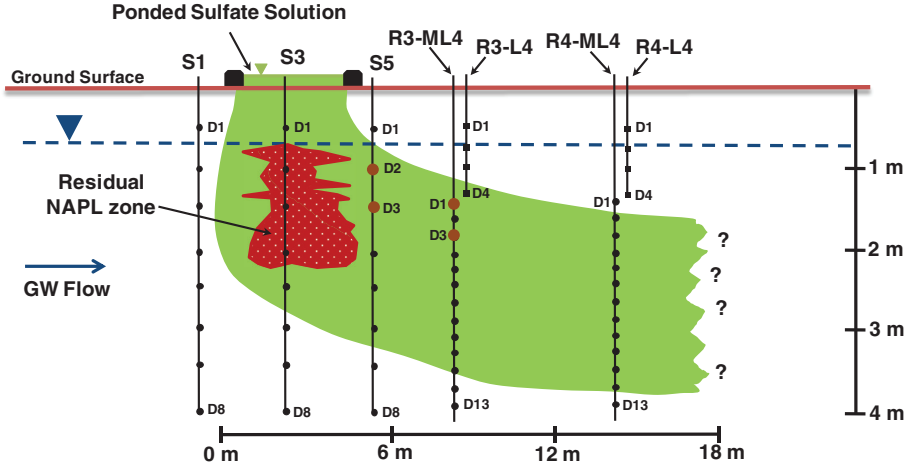

Figure 5. Longitudinal cross-section of the inferred maximum sulfate distribution extent based on the assembled data set from the three sulfate application episodes. Also shown (solid brown circles) are the four monitoring locations selected to illustrate how the suite of diagnostic tools can be applied to demonstrate enhanced sulfate reduction. The residual NAPL zone shown is a conceptual representation for illustration purposes only.

PHC Behavior

Figure 6 presents the temporal profile to Day 394 of benzene, toluene, *o*-xylene (BTX), and naphthalene at the four selected monitoring locations. Since the infiltrating sulfate solution resulted in hydraulic perturbations to the local groundwater system, changes in the concentration of PHCs observed at monitoring well S5 and R3-ML4 are potentially due to biodegradation processes, or by modifications to the groundwater flow regime that could produce an increase or decrease in the BTEX concentrations sampled.

At S5-D2 (Figure 6a), the concentration of toluene and *o*-xylene remained relatively stable following the first two sulfate application episodes, while the concentration of benzene fell from an initial value of 109 to 58 µg/L after Episode 1, and then increased to 4430 µg/L after Episode 2 before decreasing to 114 µg/L on Day 233. In contrast to the BTX concentrations at S5-D2, at S5-D3 (0.5 m deeper in the system) the BTX concentrations all decreased following Episodes 1 and 2 before slightly increasing by Day 233 (Figure 6b). The most notable was toluene which decreased from an initial value of ~7000 to 8.4 µg/L after Episode 2 before rebounding to 140 µg/L. The behavior of the BTX concentrations at both locations in R3-ML4 were similar (Figure 6c and 6d): (1) following Episode 1 the concentration of toluene and *o*-xylene decreased to <MDL, while the concentration of benzene increased significantly, (2) following Episode 2 the concentration of toluene and *o*-xylene increased to near Day −1 levels or higher by Day 103 before decreasing (more so for the levels at the deeper location R3-ML4-D3), and (3) following Episode 3 there was minor fluctuations in BTX concentrations except for a decrease in benzene concentration at R3-ML4-D3. The observed increases in some BTX concentrations following Episode 2 are most likely related to the infiltrating solution contacting residual PHCs present within the capillary fringe below the infiltration pond. Based on the changes in the BTX concentrations alone the role of biodegradation is unclear, and hence additional lines of evidence as discussed in the following sections are required to understand the behavior of this system.

Geochemical and CSIA Data

A significant decrease in Eh is observed at all four selected locations following sulfate application Episode 1 and remain low after Episode 2 (Figure 7a and 7d) indicating strong and persistent reducing conditions were created due to the applied sulfate. Sulfide concentrations also increased substantially after sulfate application Episodes 1 and 2 (Figure 7b and 7e) suggesting that sulfate reduction was enhanced. By Day 233, the sulfide concentrations remained elevated suggesting sulfate reduction was still ongoing. Low levels of methane were observed following Episode 1 and decreased to minor concentrations by Day 233 (Figure 7a and 7d) indicating that methanogenesis was not significant and sulfate-reducing conditions were present.

The rationale for the application of environmental isotopes in biodegradation studies is based on the isotopic fractionation affecting compounds involved in biogeochemical processes (Aelion et al. 2009). In the case of sulfate, during sulfate reduction the remaining sulfate gets enriched in ^{34}S as the concentration of sulfate decreases (Strebel et al. 1990). Similarly, BTX compounds get enriched in ^{13}C and ^{2}H as the concentration of these compounds decreases

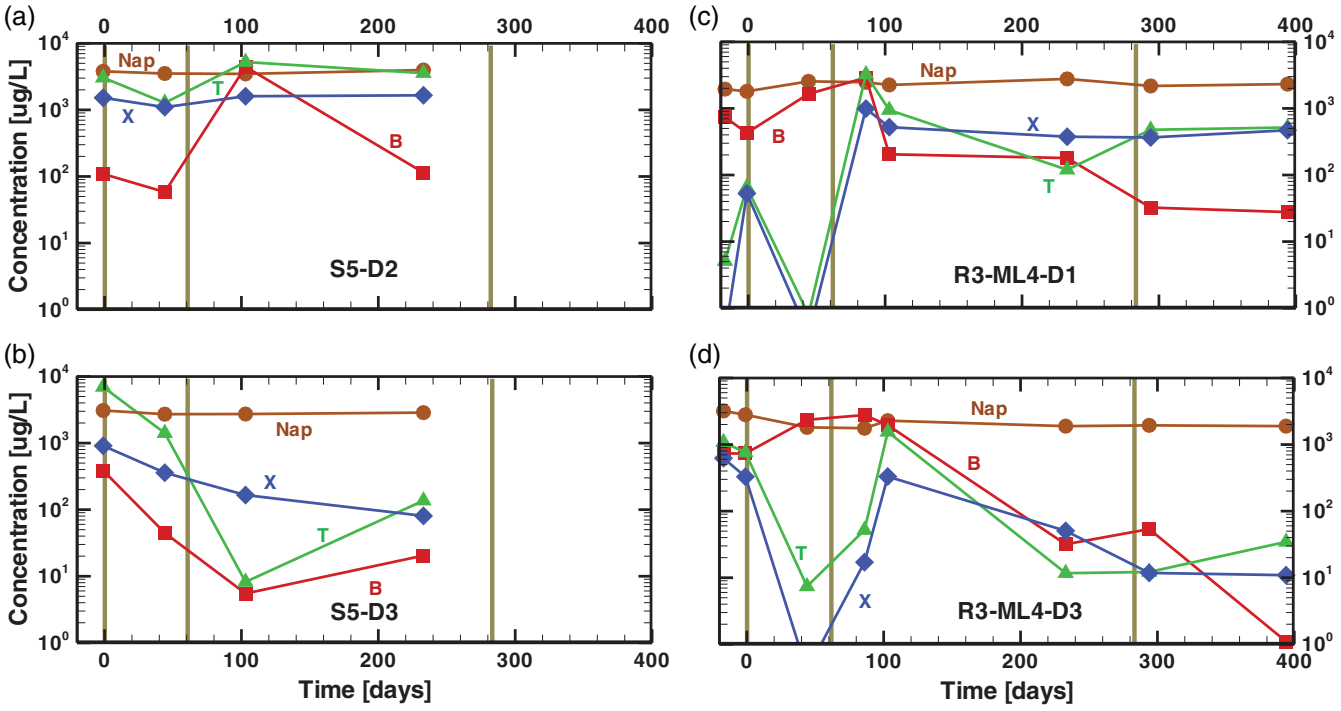

Figure 6. Temporal profile of benzene (B), toluene (T), *o*-xylene (X), and naphthalene (Nap) concentrations at monitoring location (a) S5-D2 (1.0 m bgs), (b) S5-D3 (1.5 m bgs), (c) R3-ML4-D1 (1.5 m bgs), and (d) R3-ML4-D3 (1.9 m bgs). The three sulfate application episodes are indicated with vertical brown lines at Days 0, 59, and 277.

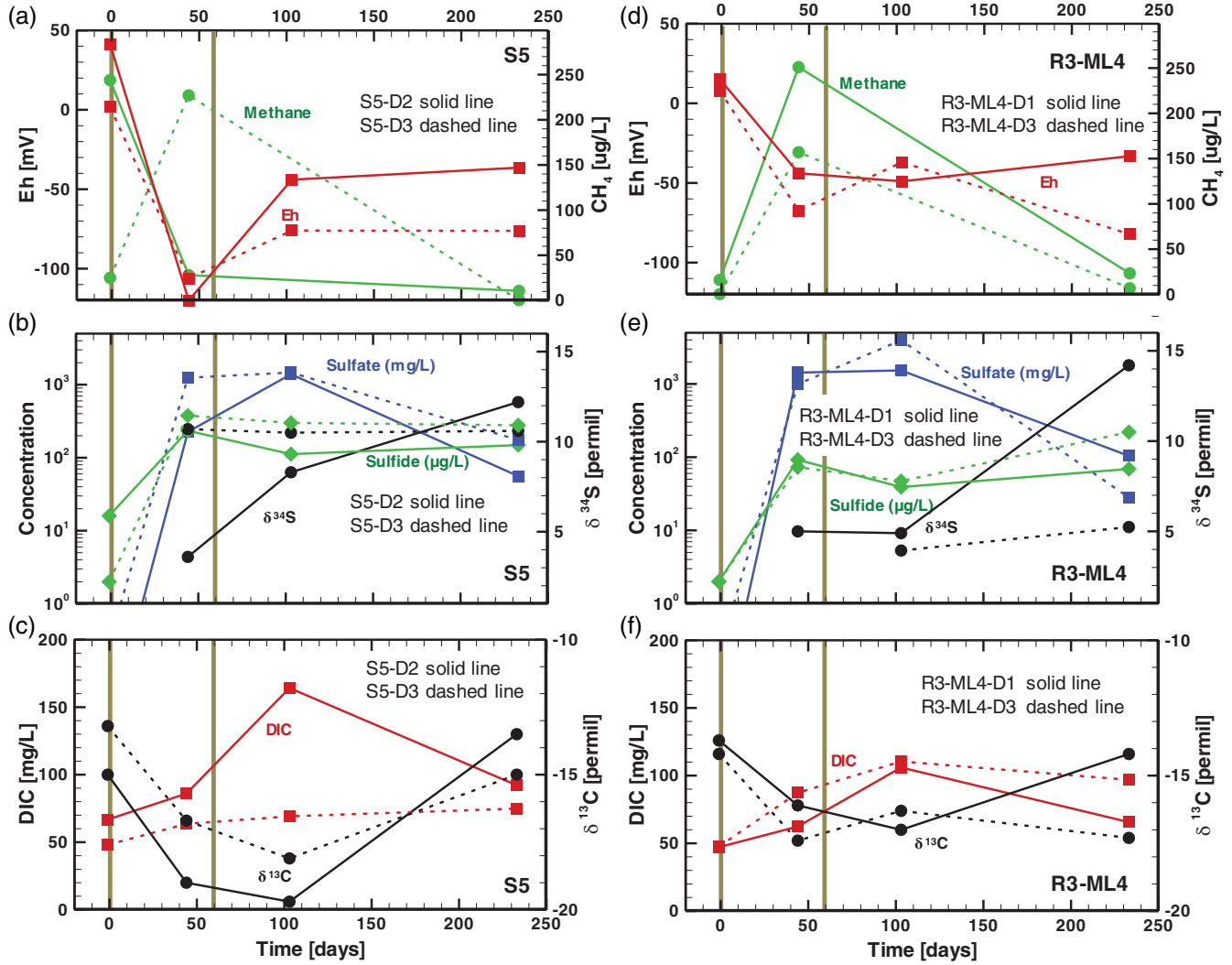

Figure 7. Temporal evolution of geochemical indicators at (a to c) S5-D2 (solid lines) and S5-D3 (dashed lines), and (d to f) R3-ML4-D1 (solid lines) and R3-ML4-D3 (dashed lines): (a, d) oxidation–reduction potential (Eh) and methane; (b, e) sulfate (mg/L), sulfide (µg/L), and $\delta^{34}S$; (c, f) DIC content in mg-C/L and $\delta^{13}C$. The sulfate application episodes are indicated with vertical brown lines at Days 0 and 59. A linear relationship was assumed for methane concentration between Days 44 and 233. The $\delta^{34}S$ value of the applied Na_2SO_4 solution was +3.2‰. The standard uncertainty is ±0.5‰ for $\delta^{13}C$ and ±0.5‰ for $\delta^{34}S$.

due to biodegradation (Hunkeler et al. 2001; Mancini et al. 2003; Meckenstock et al. 2004).

At both locations at the source well S5, the sulfate concentration increased after sulfate application Episode 1 and reached a peak concentration of ~1500 mg/L on Day 57 following Episode 2 (Figure 7b). At the shallow location (S5-D2) the $\delta^{34}S$ value (+3.6‰) at Day 44 was close to the $\delta^{34}S$ value of +3.2‰ of the applied Na_2SO_4 solution, but by Day 233 the $\delta^{34}S$ was enriched as a result of sulfate reduction to +12.2‰. At the deeper location (S5-D3), the $\delta^{34}S$ value is relatively constant at ~10‰ suggesting that sulfate-reducing conditions are enhanced due to the applied sulfate. Downgradient of the source zone at the Row 3 transect, the sulfate concentration increased in a similar pattern to that observed at S5 (Figure 7e). At both locations at R3-ML4, the $\delta^{34}S$ values were between +4 to +5‰ for the first 103 days and then shifted to more enriched values by Day 233 (as high as +15‰ at R3-ML4-D1). This enrichment was associated with a decrease in sulfate concentration (Figure 7e) and clearly indicates active sulfate reduction due to the applied sulfate.

During biodegradation, DIC is generated and the carbon isotopic composition of the DIC (DIC-$\delta^{13}C$) reflects the contribution of the organic carbon from the degraded BTX mass. In the source area at monitoring well S5 (Figure 7c), the DIC concentration increased significantly following sulfate application Episodes 1 and 2 with the concentration at the shallow location (S5-D2) reaching a value as high as 160 mg-C/L. This trend was accompanied with a shift toward more depleted DIC-$\delta^{13}C$ values of −20 and −17‰ at S5-D2 and S5-D3, respectively. By Day 233, the DIC-$\delta^{13}C$ at both locations returned toward baseline values. In contrast at the downgradient well R3-ML4, smoother patterns of DIC concentration and DIC-$\delta^{13}C$ values were observed (Figure 7f) possibly due to mixing with background water with a lower DIC concentration and more positive DIC-$\delta^{13}C$ compared to the DIC from the source zone. The DIC concentration at both locations at R3-ML4, increased to ~110 mg-C/L with a depleted DIC-$\delta^{13}C$ value of about −17‰ on Day 103. At R3-ML4-D1 the DIC concentration and DIC-$\delta^{13}C$ value by Day 233 returned to near baseline

(Day −1) conditions, while at R3-ML4-D3 there was minimal change in DIC-$\delta^{13}C$ values and DIC concentration. The observed pattern of increasing DIC concentrations associated with a shift toward more depleted DIC-$\delta^{13}C$ values was likely associated with an input of isotopically depleted DIC from biodegradation of PHCs.

CSIA for BTX

The BTX in the PHC mixture used to create the residual source zone were characterized by $\delta^{13}C$ and $\delta^{2}H$ values of −27.0 and −98‰ for benzene, −25.7 and −75‰ for toluene, and −26.0 and −97‰ for *o*-xylene, respectively. The PHC source was injected 12 months before the first sulfate application episode and some biodegradation prior to this episode can be expected to influence the isotope ratios. As shown in laboratory studies, the isotope fractionation factor for the biodegradation of BTX under sulfate-reducing conditions is smaller for carbon isotopes (−0.7 to −6.7‰) than hydrogen isotopes (−25 to −106‰) (Fischer et al. 2009; Herrmann et al. 2009; Vogt et al. 2014). This implies that a relatively large mass of these compounds would have to be removed by biodegradation to observe a shift to enriched $\delta^{13}C$ values but an appreciable shift toward enriched $\delta^{2}H$ values would be observed at lower mass loss due to biodegradation. The typical analytical uncertainty associated with $\delta^{13}C$ is ±0.5‰ and with $\delta^{2}H$ is ±7‰ inferring that enrichments larger than these values are required to confidently attribute changes to biodegradation.

Source Area: At the shallow location (S5-D2) the isotope data showed a $\delta^{13}C$ enrichment trend for benzene (−25 to −24‰) but the $\delta^{2}H$ data trended toward more depleted $\delta^{2}H$ values (−29 to −89‰) followed by a shift toward an enriched $\delta^{2}H$ value of −31‰ by Day 233 (Figure 8a and 8b). The shift toward more depleted $\delta^{2}H$ values was accompanied by a significant increase in benzene concentration (Figure 6a) following sulfate application Episode 2. When the benzene concentration returned to near baseline (Day −1) levels the shift was toward more enriched $\delta^{2}H$ values. Despite the benzene concentration increasing significantly after Episode 2, the $\delta^{2}H$ value never returned to the source benzene value of −98‰ implying that some benzene mass was being removed by biodegradation. For toluene, the carbon isotope data showed a shift toward enriched $\delta^{13}C$ values (−26.3 to −24.6‰, Figure 8a) reaching a peak value after sulfate application Episode 2. Similar to $\delta^{13}C$, the $\delta^{2}H$ data for toluene showed a shift toward more enriched $\delta^{2}H$ values (−70 to −53‰) (Figure 8b). This toluene isotope pattern was accompanied with a trend toward decreasing concentration after Episode 1 and, similar to benzene, the toluene concentration increased after Episode 2 and then decreased reaching 3600 µg/L at Day 233 (Figure 6a). For *o*-xylene, the isotope data showed no appreciable shift for $\delta^{13}C$ values (Figure 8a) but $\delta^{2}H$ was enriched (−97.5 to −81‰) after Episode 2 (Figure 8b).

At the deeper location (S5-D3) a different isotope pattern than appeared at S5-D2 was observed. No appreciable $\delta^{13}C$ changes were detected for benzene with values around −25‰ (Figure 8c). However, the $\delta^{2}H$ for benzene showed a clear shift toward more enriched values after Episodes 1 and 2 (−87 to −63 and then −72‰) (Figure 8d). This isotope pattern was accompanied by a significant decrease in benzene concentration (4200 to 25 µg/L) (Figure 6b). A large $\delta^{13}C$ isotope shift in toluene was observed after Episode 2 (−25.5 to −21.4‰) and then a return to −25.5‰ at Day 233 (Figure 8c). The hydrogen isotope data for toluene also showed a shift toward more enriched $\delta^{2}H$ values (−72 to −54‰, Figure 8d) but unfortunately data was not available on Day 44 or Day 233 as toluene concentrations were lower than the reporting limit for CSIA. Similar, to the benzene isotope pattern, the toluene isotope pattern was accompanied by a significant decrease in toluene concentration (Figure 6b). The isotope pattern for *o*-xylene showed enrichment following Episode 2 for both $\delta^{13}C$ (−25.6 to −24.2‰) and $\delta^{2}H$ (−81 to −51‰) (Figure 8c and 8d). By Day 233 the $\delta^{13}C$ value for *o*-xylene returned to near Day −1 values while $\delta^{2}H$ remained enriched. This *o*-xylene isotope pattern was also accompanied by a decrease in the *o*-xylene concentration (Figure 6b).

Downgradient Transect: At the shallow location at Row 3 (R3-ML4-D1) the $\delta^{13}C$ in benzene showed a trend of depleted values from −23.8 to −24.8‰ and then increasing to −24.1‰ at Day 233 (Figure 8e). A similar trend was observed for the $\delta^{2}H$ values which changed from −58 to −84‰ and then increased to −31‰ at Day 233 (Figure 8f). Toluene also showed a trend toward more depleted $\delta^{13}C$ values after Episode 2 from −24.2 to −25.6‰ and then an increase to −25.1‰ at Day 233. A similar pattern was observed for the $\delta^{2}H$ in toluene changing from −27 to −60‰ and then increasing to −41‰ at Day 233 (Figure 8f). Similar to benzene and toluene, the $\delta^{13}C$ data for *o*-xylene showed a depleting trend from −26.4 to −25.8‰ and −25.7‰ at Day 233 (Figure 8e). The $\delta^{2}H$ data also showed a depletion trend from −71 to −89‰ and increasing to −67‰ at Day 233 (Figure 8f). These isotope patterns for BTX were all accompanied by a spike in the BTX concentrations after sulfate application Episode 2 followed by decreasing concentrations to Day 233 (Figure 6c).

At the deeper location (RM3-ML4-D3) the $\delta^{13}C$ values in benzene showed a small trend toward depleted values (−24.3 to −24.8‰) after Episode 2 (Figure 8g) while $\delta^{2}H$ trend toward depleted values from −55 to −79‰ and then an enrichment toward −56‰ (Figure 8h). The changes in $\delta^{13}C$ values for toluene were also small (−24.4 to −25‰) but the $\delta^{2}H$ showed a shift toward more enriched values from −69 to −32‰ after Episode 2. The pattern of $\delta^{13}C$ in *o*-xylene was similar to benzene and toluene, with a shift toward depleted values (−24.8 to −25.8‰) after Episode 2 and then to −25.3‰ at Day 233. The $\delta^{2}H$ in *o*-xylene varied between −78 and −72‰ after Episode 2 and reached an enriched value of −42‰ at Day 233 (Figure 8h). Similar to the behavior at the shallow location, these isotope patterns were accompanied by an increase in the BTX concentrations after sulfate application Episode 2 followed by decreasing concentrations (Figure 6d).

Synopsis: The increase in BTX concentrations following Episode 2 was likely related to the infiltrating solution contacting residual PHCs present within the capillary fringe.

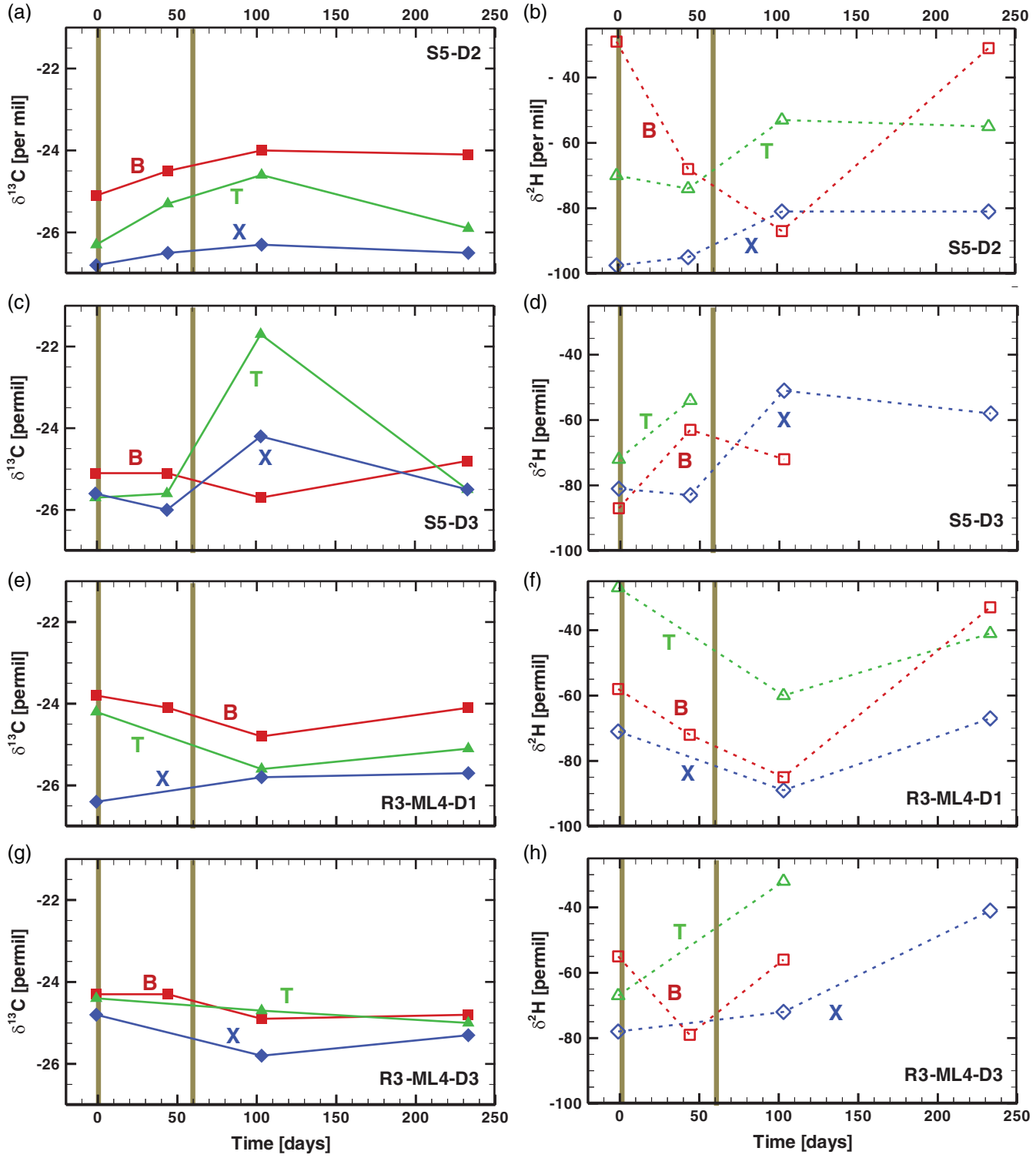

Figure 8. Temporal evolution of $\delta^{13}C$ (solid line with filled symbols) and $\delta^{2}H$ (dashed line with open symbols) of benzene (B, red), toluene (T, green), and *o*-xylene (X, blue) at monitoring location (a, b) S5-D2 (1.0 m bgs), (c, d) S5-D3 (1.5 m bgs), (e, f) R3-ML4-D1 (1.5 m bgs), and (g, h) R3-ML4-D3 (1.9 m bgs). The sulfate application episodes are indicated with vertical brown lines at Days 0 and 59. Where data were missing at Day 44 a linear relationship was assumed. The $\delta^{13}C$ and $\delta^{2}H$ values of the PHC source were −27.0 and −98‰ for benzene, −25.7 and −75‰ for toluene, and −26.0 and −97‰ for *o*-xylene, respectively.

The BTX isotopic signature was similar to the residual source isotopic signature. The more enriched isotope values observed at Day −1 at S5-D3, R3-ML4-D1, and R3-ML4-D3 compared to the signature of the BTX in the residual source indicates that these compounds were being biodegraded prior to the first sulfate application episode. The enriched isotope patterns for BTX observed during the sulfate application episodes, even when the concentration increased after Episode 2, indicates that benzene, toluene and to a lesser degree *o*-xylene were being biodegraded which is consistent with the isotope and concentration patterns observed for DIC (Figure 7c and 7f).

Biomarkers

At all four locations (the source monitoring well S5, and R3-ML4), toluene *cis*-dihydrodiol and benzene *cis*-dihydrodiol (signature metabolites of aerobic biodegradation of toluene and benzene, respectively) were not detected (data not shown). Expression of *todC* (aromatic dioxygenase, encoding aerobic biodegradation of toluene) was not detected (<100 copies/L) throughout the experiment at both S5-D3 and R3-M4-D3 consistent with the strong reducing conditions (Figure 7a and 7d). At the shallower depths (S5-D2, and R3-M4-D1) there were occasional detections of mRNA of the *todC* as high as ~553,000 copies/L. This was likely associated with the mixing of the oxygen-rich infiltrating solution with the PHC laden groundwater.

Figure 9 shows the evolution of biomarkers observed at R3-M4-D1 and R3-M4-D3 that are unique to anaerobic biodegradation of aromatics or sulfate reduction (*abcA* mRNA, *bssA*-SRB mRNA, *dsrB* mRNA, and benzylsuccinates). Unfortunately, the anaerobic biomarker data set assembled at the source well S5 was sporadic as a result of some sampling and handling issues, and hence these data are not presented or discussed.

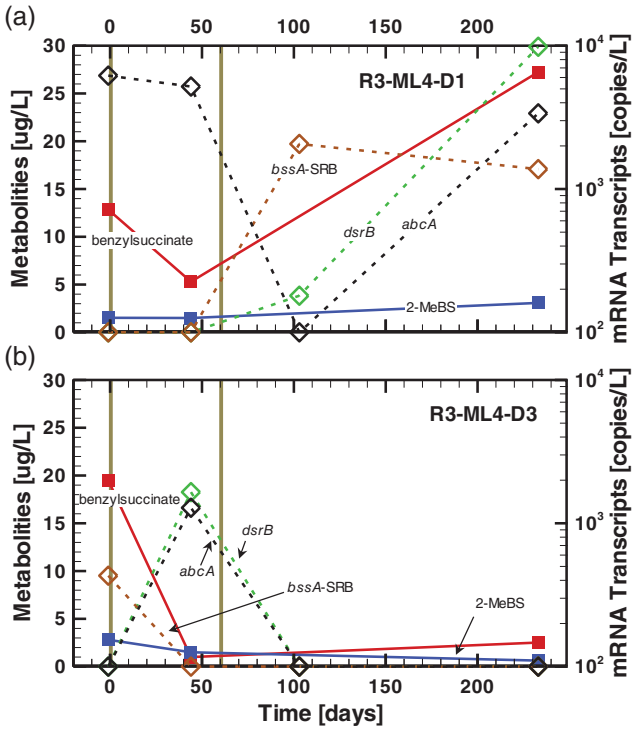

Figure 9. Temporal patterns in the appearance of biomarkers (mRNA and metabolites) at (a) R3-ML4-D1 and (b) R3-ML4-D3. Shown are metabolites benzylsuccinate and 2-MeBS (2-methyl benzylsuccinate) unique to anaerobic biodegradation of toluene and xylene, respectively; and *abcA* (anaerobic benzene carboxylase) mRNA active in anaerobic benzene metabolism, *bssA*-SRB (benzylsuccinate synthase) mRNA active in anaerobic toluene metabolism under sulfate-reducing conditions, and *dsrB* (dissimilatory sulfate reductase) mRNA linked to the reduction of sulfate in anaerobic conditions. The sulfate application episodes are indicated with vertical brown lines at Days 0 and 59. Where data were missing at Day 103 a linear relationship was assumed.

At R3-M4-D1 the transcripts and metabolites for toluene and *o*-xylene degradation were initially below detection, but increased after sulfate application Episode 2 and followed the same trend as *dsrB* expression. These increased levels are suggestive of ongoing anaerobic biodegradation of toluene and *o*-xylene which is consistent with the CSIA data. The increase in *dsrB* by Day 233 mirrors the enrichment pattern for ^{34}S in sulfate (Figure 7e) and carbon and hydrogen isotope values for BTX over the same period (Figure 8e and 8f). Interestingly, transcripts of *abcA* were initially high, but decreased after sulfate application Episode 2 and were opposite in trend to *bssA*-SRB. Despite this, there was a substantial decrease in the toluene/benzene ratio (Figure 6c) suggesting that toluene was being degraded at a faster rate than benzene, even though *bssA*-SRB transcript levels were low (Wilson et al. 2016).

At R3-M4-D3 the magnitude of transcripts and metabolite concentrations for toluene and *o*-xylene were substantially lower than observed at the shallower location (R3-M4-D1). For example on Day 233, the concentration of benzylsuccinate unique to anaerobic biodegradation of toluene was an order-of-magnitude lower (2.5 vs. 27 µg/L) despite CSIA evidence of biodegradation. An inverse correlation between the presence of *bssA*-SRB and *abcA* is also observed. The levels of *bssA*-SRB were at their highest just prior to Episode 1 and then fell to <MDL for the remainder of the experiment. Expression of *abcA* and *dsrB* mirrored one another: initially they were <MDL, spiking after Episode 1, but then dropped again to <MDL where they remained for the duration of the experiment. An increase was observed in *dsrB* transcripts after the first injection decreasing to values <MDL after sulfate application Episode 2, which seemed to be consistent with small enrichment in $\delta^{34}S$ (Figure 7e) values, however the concentration and isotope patterns for DIC (Figure 7f) and isotope patterns for BTX (Figure 8g and 8h) indicated that biodegradation was active in the deeper part of the aquifer at R3-M4. Similar to the shallower depth, the toluene/benzene ratio (Figure 6d) dipped dramatically, but transiently after the first sulfate addition which suggested toluene degradation exceeded benzene degradation.

The detection of metabolites specific to toluene and *o*-xylene biodegradation by SRB (benzylsuccinate and 2-methylbenzylsuccinate) and expression of the genes encoding the enzymes responsible for their production is evidence of biodegradation. These detections were observed despite additional BTX mass entering the system due to the hydraulic perturbations caused by the three infiltration episodes. This was particularly true of *abcA* expression which was highest at both locations despite drops in the toluene/benzene ratio.

Closure

In this pilot-scale experiment a surface-based delivery method was used to episodically apply sulfate into a residual PHC zone. While the surficial infiltration pond was useful to control sulfate application volume, concentration, timing, and overall residence time of sulfate in the residual PHC zone, the migration of sulfate was primarily controlled by density-dependent advection. In general, the

sulfate-enriched water left the infiltration pond and mixed with upgradient groundwater as it migrated downward through the residual PHC zone and by ~8 m downgradient had reached a depth of ~3.7 m bgs. The empirical attempts employed to minimize density effects while ensuring that a nominal mass of sulfate was delivered were unsuccessful to control the sinking of the infiltration sulfate solution. However, for the purpose of this experiment, sufficient sulfate mass was delivered to increase sulfate concentrations to sustain enhanced sulfate reduction at the downgradient monitoring locations.

The hydraulic perturbations to the system as a result of the sulfate infiltration episodes resulted in some observed increases in BTX concentrations. This additional input of BTX mass into the saturated system is presumed to be related to the infiltrating solution contacting residual PHCs present within the capillary fringe below the infiltration pond. Hence the ability to use BTX concentration profiles alone to indicate that enhanced biodegradation occurred as a result of the applied sulfate was not possible. Although confounded by the input of BTX mass, geochemical, CSIA and biomarker data provided additional lines of evidence to support the presence of enhanced sulfate reduction following sulfate application and biodegradation of BTX (Table 1). Specifically, sulfate was enriched in ^{34}S, the DIC produced was depleted in ^{13}C, enriched C and H isotope patterns were observed for BTX, metabolites specific to toluene and *o*-xylene biodegradation by SRB were detected, and the expression of the genes encoding the enzymes responsible for the production of these metabolites were present.

Table 1
Summary of Increasing Lines of Evidence to Support the Occurrence of Enhanced Sulfate Reduction

	Monitoring Tool	Observations
✖	BTX concentrations	Variable; inconclusive trends
✓	Dissolved oxygen (DO)	Minimal (<1 mg/L); anoxic conditions
✓	Redox potential (Eh)	Decreased values; reducing conditions present
✓	Sulfide	Elevated levels; sulfate reduction ongoing
✓	Methane (CH_4)	Low levels; methanogenesis not significant
✖	Sulfate (SO_4^{2-})	Increasing then decreasing values
✓	Sulfur (^{34}S) isotopic composition of sulfate	Enriched values; sulfate reduction
✓	Dissolved inorganic carbon (DIC)	Increased concentration; PHC mineralization
✓	Carbon isotopic composition of DIC (DIC-$\delta^{13}C$)	Depleted values; contribution from degraded BTX mass
✓	Carbon ($\delta^{13}C$) and hydrogen ($\delta^{2}H$) isotopic composition of BTX (CSIA)	Enriched $\delta^{13}C$ and $\delta^{2}H$ patterns observed for BTX
✓	Metabolites of microbial origin	Metabolites specific to toluene and *o*-xylene biodegradation by SRB detected
✓	mRNA of biodegradation genes	Genes encoding the enzymes responsible for BTX biodegradation and sulfate reduction present

While the results of this pilot-scale investigation provided insight into some factors controlling surface-based delivery of sulfate to shallow impacted groundwater systems, there are still many unanswered questions (e.g., controls on dissolution of solid sulfate salts, preferential pathways in the unsaturated zone, sulfate demand exerted by PHCs near the capillary fringe, and mixing within PHC plumes) surrounding basic design parameters and ways to optimize mass removal performance under dynamic conditions. We believe that a combination of conventional monitoring tools augmented with isotopic and molecular-biological procedures which provide additional lines of evidence will lead to a better understanding of this cost-effective approach to enhance biodegradation of PHCs.

Acknowledgments

Financial support for this investigation was provided by Chevron Energy Technology Company, American Petroleum Institute (API), and a NSERC of Canada Collaborative Research and Development grant (N.R.T.). We thank Anthony Hay for his assistance with the biomarker data, and John Wilson, Peter Bennet, Elizabeth Edwards and Matthew Schnobrich for their helpful comments on this manuscript.

Supporting Information

Appendix S1. Analytical methods.

Figure S1. UVOST profile collected from the residual PHC source zone.

Figure S2. Correlation between sulfate (mg/L) and electrical conductivity (EC).

Table S1. Composition of injected PHC NAPL.

Table S2. PCR primers.

References

Abu Laban, N., D. Selesi, T. Rattei, P. Tischler, and R.U. Meckenstock. 2010. Identification of enzymes involved in anaerobic benzene degradation by a strictly anaerobic iron-reducing enrichment culture. *Environmental Microbiology* 12, no. 10: 2783–2796.

Aelion, C.M., P. Iochener, D. Hunkeler, and R. Aravena. 2009. *Environmental Isotopes in Biodegradation and Bioremediation*. Boca Raton, Florida: Taylor & Francis Group, LLC.

Anderson, R., and D. Lovley. 2000. Anaerobic bioremediation of benzene under sulfate-reducing conditions in a petroleum-contaminated aquifer. *Environmental Science & Technology* 34: 2261–2266.

Atlas, R.M. 1981. Microbial degradation of petroleum hydrocarbons: An environmental perspective. *Micro-biological Reviews* 45, no. 1: 180–209.

Baedecker, M.J., R.P. Eganhouse, H. Qi, I.M. Cozzarelli, J.J. Trost, and B.A. Bekins. 2018. Weathering of oil in surficial aquifer. *Ground Water* 56: 797–809. https://doi.org/10.1111/gwat.12619

Bekins, B.A., F.D. Hostettler, W.N. Herkelrath, G.N. Delin, E. Warren, and H.I. Essaid. 2005. Progression of methanogenic degradation of crude oil in the subsurface. *Environmental Geosciences* 12, no. 2: 139–152.

Beller, H.R., S.R. Kane, T.C. Legler, J.R. McKelvie, B.S. Lollar, F. Pearson, L. Balser, and D.M. Mackay. 2008. Comparative assessments of benzene, toluene, and xylene natural attenuation by quantitative polymerase chain reaction analysis of a catabolic gene, signature metabolites, and compound-specific isotope analysis. *Environmental Science & Technology* 42, no. 16: 6065–6072.

Beller, H.R., A.M. Spormann, P.K. Sharma, J.R. Cole, and M. Reinhardt. 1996. Isolation and characterization of a novel toluene-degrading, sulfate-reducing bacterium. *Applied and Environmental Microbiology* 62, no. 4: 1188–1196.

Bourne, D.G., A. Muirhead, and Y. Sato. 2011. Changes in sulfate reducing bacterial populations during the onset of black band disease. *ISME Journal* 5, no. 3: 559–564.

Cébron, A., M.P. Norini, T. Beguiristain, and C. Leyval. 2008. Real-time PCR quantification of PAH-ring hydroxylating dioxygenase (PAH-RHD α) genes from gram positive and gram negative bacteria in soil and sediment samples. *Journal of Microbiology Methods* 73, no. 2: 148–159.

Chapelle, F.H. 1999. Bioremediation of petroleum hydrocarbon-contaminated ground water: The perspectives of history and hydrology. *Ground Water* 37, no. 1: 122–132.

Chin, K.J., M.L. Sharma, L.A. Russell, K.R. O'Neill, and D.R. Lovley. 2008. Quantifying expression of a dissimilatory (bi)sulfite reductase gene in petroleum-contaminated marine harbor sediments. *Microbial Ecology* 55, no. 3: 489–499.

Cunningham, J.A., H.A. Rahme, G.D. Hopkins, C. Lebron, and M. Reinhard. 2001. Enhanced in situ bioremediation of BTEX-contaminated groundwater by combined injection of nitrate and sulfate. *Environmental Science & Technology* 35: 1663–1670.

Diaz, E., J.I. Jiménez, and J. Nogales. 2013. Aerobic degradation of aromatic compounds. *Current Opinion in Biotechnology* 24, no. 3: 431–442.

Fischer, A., M. Gehre, J. Breitfeld, and C. Vogt. 2009. Carbon and hydrogen isotope fractionation of benzene during biodegradation under sulfate-reducing conditions: A laboratory to field site approach. *Rapid Comunication in Mass Spectrometry* 23: 2439–2447.

Foght, J. 2008. Anaerobic biodegradation of aromatic hydrocarbons: Pathways and prospects. *Journal of Molecular Microbiology and Biotechnology* 15: 93–120.

Freitas, J.G., and J.F. Barker. 2008. Sampling VOCs with porous suction samplers in the presence of ethanol: How much are we losing? *Ground Water Monitoring & Remediation* 28, no. 3: 83–92.

Freitas, J.G., M.T. Mocanu, J.L.G. Zoby, J.W. Molson, and J.F. Barker. 2011. Migration and fate of ethanol-enhanced gasoline in groundwater: A modeling analysis of a field experiment. *Journal of Contaminant Hydrology* 119: 25–43.

Fuchs, G., M. Boll, and J. Heider. 2011. Microbial degradation of aromatic compounds from one strategy to four. *Nature Review Microbiology* 9, no. 11: 803–816.

Geets, J., B. Borremans, L. Diels, D. Springael, J. Vangronsveld, D. van der Lelie, and K. Vanbroekhoven. 2006. DsrB gene-based DGGE for community and diversity surveys of sulfate-reducing bacteria. *Journal of Microbiological Methods* 66: 194–205.

Gülensoy, N., and P.J. Alvarez. 1999. Diversity and correlation of specific aromatic hydrocarbon biodegradation capabilities. *Biodegradation* 10, no. 5: 331–340.

Harms, G., K. Zengler, R. Rabus, F. Aeckersberg, D. Minz, R. Rosselló-Mora, and F. Widdel. 1999. Anaerobic oxidation of o-xylene, m-xylene, and homologous alkylbenzenes by new types of sulfate-reducing bacteria. *Applied and Environmental Microbiology* 65, no. 3: 999–1004.

Hendrickx, B.H., H. Junca, J. Vosahlova, A. Lindner, I. Ruegg, M. Bucheli-Witschel, F. Faber, T. Egli, M. Mau, D.H. Pieper, E.M. Top, W. Dejonghe, L. Bastiaens, and D. Springael. 2006. Alternative primer sets for PCR detection of genotypes involved in bacterial aerobic BTEX degradation: Distribution of the genes in BTEX degrading isolates and in subsurface soils of a BTEX contaminated industrial site. *Journal of Microbiology Methods* 64, no. 2: 250–265.

Herrmann, S., C. Vogt, A. Fischer, A. Kuppardt, and H.H. Richnow. 2009. Characterization of anaerobic xylene biodegradation by two-dimensional isotope fractionation analysis. *Environmental Microbiology Report* 1, no. 6: 535–544.

Hunkeler, D., N. Andersen, R. Aravena, S.M. Bernasconi, and B.J. Butler. 2001. Hydrogen and carbon isotopic fractionation during aerobic biodegradation of benzene. *Environmental Science & Technology* 35: 3462–3467.

Hutchins, S.R., and D.E. Miller. 1998. Combined laboratory/field study on the use of nitrate for in situ bioremediation of a fuel-contaminated aquifer. *Environmental Science & Technology* 32: 1832–1840.

Kazy, S.K., A.L. Monier, and P.J.J. Alvarez. 2010. Assessing the correlation between anaerobic toluene degradation activity and bssA concentrations in hydrocarbon-contaminated aquifer material. *Biodegradation* 21, no. 5: 793–800.

Kleikemper, J., M.H. Schroth, W.V. Sigler, M. Schmucki, S.M. Bernasconi, and J. Josef Zeyer. 2002. Activity and diversity of sulfate-reducing bacteria in a petroleum hydrocarbon-contaminated aquifer. *Applied and Environmental Microbiology* 68, no. 4: 1516–1523.

Kolhatkar, R., and M. Schnobrich. 2017. Land application of sulfate salts for enhanced natural attenuation of benzene in groundwater: A case study. *Groundwater Monitoring & Remediation* 37, no. 2: 43–57.

Kolhatkar, A., L. Bruce, R. Kolhatkar, S. Flagel, D. Beckmann, and E. Larsen. 2008. Harnessing sulfate-reducing microbial ecology to enhance attenuation of dissolved BTEX at two petroleum-impacted sites. *Ecological Chemistry and Engineering* 15, no. 6: 535–548.

Leahy, J.G., and R.R. Colwell. 1990. Microbial degradation of hydrocarbons in the environment. *Microbiological Reviews* 52, no. 3: 305–315.

Lunardini, R.C. Jr., and R.L. Dickey III. 2003. Enhanced anaerobic bioremediation of petroleum hydrocarbons in groundwater using sulfate. In *Proceedings of the Seventh International In Situ and On-Site Bioremediation Symposium*, ed. V.S. Magar, and M.E. Kelley. Columbus, Ohio: Battelle Press.

MacFarlane, D.S., J.A. Cherry, R.W. Gilham, and E.A. Sudicky. 1983. Migration of contaminants in groundwater at a NDFILL: A case-groundwater flow and plume delineation. *Journal of Hydrology* 63, no. 1–2: 1–29.

Mackay, D.M., D.L. Freyberg, P.V. Roberts, and J.A. Cherry. 1986. A natural gradient experiment on solute transport in a sand aquifer: 1. Approach and overview of plume movement. *Water Resources Research* 22, no. 13: 2017–2029.

Mancini, S.A., A.C. Ulrich, G. Lacrampe-Couloume, B. Sleep, E.A. Edwards, and B. Sherwood Lollar. 2003. Carbon and hydrogen isotopic fractionation during anaerobic biodegradation of benzene. *Applied and Environmental Microbiology* 69: 191–198.

McGuire, J.T., D.T. Long, and D.W. Hyndman. 2005. Analysis of recharge-induced geochemical change in a contaminated aquifer. *Ground Water* 43, no. 4: 518–530.

Meckenstock, R.U., and H. Mouttaki. 2011. Anaerobic degradation of non-substituted aromatic hydrocarbons. *Current Opinion in Biotechnology* 22: 406–414.

Meckenstock, R.M., M. Elsner, C. Griebler, T. Lueders, C. Stumpp, J. Aamand, S.N. Agathos, H. Albrechtsen, L. Bastiaens, P.L. Bjerg, N. Boon, W. Dejonghe, W.E. Huang, S.I. Schmidt, E. Smolders, S.R. Sørensen, D. Springael, and B.M. van Breukelen. 2015. Biodegradation: Updating the concepts of control for microbial cleanup in contaminated aquifers. *Environmental Science & Technology* 49: 7073–7081.

Meckenstock, R.U., B. Morasch, C. Gribler, and H.H. Richnow. 2004. Stable isotope fractionation analysis as a tool to monitor biodegradation in contaminated aquifers. *Journal of Contaminant Hydrology* 75: 215–255.

Molson, J.W., and E.O. Frind. 2013. *SALTFLOW Version 3.0 User Guide, Density-Dependent Flow and Mass Transport Model in Three Dimensions*. Waterloo, Ontario, Canada: Department of Earth Science, University of Waterloo.

Nebe, J., B.R. Baldwin, R.L. Kassab, L. Nies, and C.H. Nakatsu. 2009. Quantification of aromatic oxygenase genes. *Environmental Science & Technology* 43, no. 6: 2029–2034.

Neretin, L.N., A. Schippers, A. Pernthaler, K. Hamann, R. Amann, and B.B. Jørgensen. 2003. Quantification of dissimilatory (bi) sulphite reductase gene expression in Desulfobacterium autotrophicum using real-time RT-PCR. *Environmental Microbiology* 5, no. 8: 660–671.

Pelikan, C., C.W. Herbold, B. Hausmann, A.L. Müller, M. Pester, and A. Loy. 2016. Diversity analysis of sulfite- and sulfate reducing microorganisms by multiplex dsrA and dsrB amplicon sequencing using new primers and mock community-optimized bioinformatics. *Environment Microbiology* 18, no. 9: 2994–3009.

Roychoudhury, A.N., and D.W. McCormick. 2006. Kinetics of sulfate reduction in a coastal aquifer contaminated with petroleum hydrocarbons. *Biogeochemistry* 81: 17–31.

van Stempvoort, D.R., J. Armstrong, and B.F. Mayer. 2007. Seasonal recharge and replenishment of sulfate associated with biodegradation of a hydrocarbon plume. *Groundwater Monitoring & Remediation* 27, no. 4: 110–121.

Strebel, O., J. Boettcher, and P. Fritz. 1990. Use of isotope fractionation of sulfate-sulfur and sulfate-oxygen to assess bacterial desulfurication in a sandy aquifer. *Journal of Hydrology* 121: 155–172.

Sublette, K., A. Peacock, D. White, G. Davis, D. Ogles, D. Cook, R. Kolhatkar, D. Beckmann, and X. Yang. 2006. Monitoring subsurface microbial ecology in a sulfate-amended, gasoline-contaminated aquifer. *Ground Water Monitoring & Remediation* 26, no. 2: 70–78.

Suthersan, S., K. Houston, M. Schnobrich, and J. Horst. 2011. Engineered anaerobic bio-oxidation systems for petroleum hydrocarbon residual source zones with soluble sulfate application. *Ground Water Monitoring & Remediation* 31, no. 3: 41–46.

U.S. Environmental Protection Agency (U.S. EPA). 2007. *Monitored Natural Attenuation of Tertiary Butyl Alcohol (TBA) at Gasoline Spill Sites*. EPA/600/R-07/10e0. Washington, DC: U.S. EPA.

Vogt, C., C. Dorer, S. Kimmel, P. Bombach, A. Fischer, and H.H. Richnow. 2014. Monitoring BTEX degradation by CSIA chances and challenges. In *EGU General Assembly, April 27-May 2*. Vienna, Austria: EGU.

Wiedemeier, T.H., H.S. Rifai, C.J. Newell, and J.T. Wilson. 1999*Natural Attenuation of Fuels and Chlorinated Solvents in the Subsurface*. New York: John Wiley and Sons.

Wilson, M.S., and E.L. Madsen. 1996. Field extraction of a unique intermediary metabolite indicative of real time in situ pollutant biodegradation. *Environmental Science & Technology* 30, no. 6: 2099–2103.

Wilson, J.T., C. Adair, H. White, and R.L. Howard. 2016. Effect of biofuels on biodegradation of benzene and toluene at gasoline spill sites. *Groundwater Monitoring & Remediation* 36, no. 4: 50–61.

Biographical Sketches

***Yunxiao Wei**, M.Sc, is at BCEG Environmental Remediation Co., Ltd., Beijing, China and Ph.D. candidate in the Department of Civil and Environmental Engineering, University of Waterloo, 200 University Avenue West, Waterloo N2L 3G1, ON, Canada.*

***Neil R. Thomson**, Ph.D., P.Eng., corresponding author, is Professor in the Department of Civil and Environmental Engineering, University of Waterloo, 200 University Avenue West, Waterloo N2L 3G1, ON, Canada; neil.thomson@uwaterloo.ca*

***Ramon Aravena**, Ph.D., is Emeritus and Adjunct Professor in the Department of Earth and Environmental Sciences, University of Waterloo, 200 University Avenue West, Waterloo N2L 3G1, ON, Canada.*

***Massimo Marchesi**, Ph.D., is Postdoctoral Fellow in the Department of Civil and Environmental Engineering, University of Waterloo, Waterloo, ON, Canada and now a Research Fellow at Politecnico di Milano, Department of Civil and Environmental Engineering, 32 Piazza L. Da Vinci, Milano 20133, Italy.*

***James F. Barker**, Ph.D., is Emeritus and Adjunct Professor in the Department of Earth and Environmental Sciences, University of Waterloo, 200 University Avenue West, Waterloo N2L 3G1, ON, Canada.*

***Eugene L. Madsen**, Ph.D., Deceased, was Professor in the Department of Microbiology, Cornell University, 123 Wing Drive, Ithaca, NY 14853.*

***Ravi Kolhatkar**, Ph.D., M.B.A., is Senior Staff Hydrogeologist in the Health, Environment, and Safety Department, Chevron Energy Technology Company, 1200 Smith St., Houston, TX 77002.*

***Tim Buscheck**, M.Sc., is Chevron Fellow and Senior Consulting Hydrogeologist in the Health, Environment, and Safety Department, Chevron Energy Technology Company, 6001 Bollinger Canyon Road, San Ramon, CA 94583.*

***Daniel Hunkeler**, Ph.D., is Professor and Director of the Centre for Hydrogeology and Geothermics (CHYN), University of Neuchâtel, Switzerland and Adjunct Professor, Department of Earth and Environmental Sciences, University of Waterloo, Waterloo N2L 3G1, ON, Canada.*

***Christopher M. DeRito**, M.S., is Research Support Specialist in the Department of Microbiology, Cornell University, 125 Wing Drive, Ithaca, NY 14853.*